Received: 21 July 2023 | Revised: 1 February 2024 | Accepted: 2 February 2024

DOI: 10.1002/nano.202300111

RESEARCH ARTICLE

nano select Open Access WILEY

Porous silicon nanotube bundles as nanocarriers for small interfering RNA delivery

Nguyen T. Le[1] | **Giridhar R. Akkaraju**[2] | **Jeffery L. Coffer**[1]

[1]Department of Chemistry and Biochemistry, Texas Christian University, Fort Worth, Texas, USA

[2]Department of Biology, Texas Christian University, Fort Worth, Texas, USA

Correspondence
Jeffery L. Coffer, Department of Chemistry and Biochemistry, Texas Christian University, Fort Worth, TX 76129, USA.
Email: j.coffer@tcu.edu

Funding information
Robert A. Welch Foundation, Grant/Award Number: P-1212

Abstract

We describe in this work an evaluation of bundles of hollow mesoporous silicon nanotubes to facilitate transfection of HeLa cells using small interfering RNA designed to knock down expression of Enhanced Green Fluorescent Protein (eGFP). These experiments entail direct visualization of the nanotube bundles associated with the cells using both scanning electron microscopy (SEM) and confocal fluorescence imaging. These nanotube bundles are generated by surface modification of nanotube arrays with aminopropyl-triethoxysilane (APTES), followed by their ultrasonication in water, to create the amine-terminated structures capable of electrostatic conjugation of siRNA at an efficiency of 23%–50% (depending on initial siRNA concentration). Delivery and transfection to HeLa cells are verified by quantification of fluorescence imaging; an average percent knockdown of ~50% eGFP is achieved. As nanoscale drug delivery vehicles are expected to be resorbed in clinical use, we also assess SiNT bundle degradation during the above in vitro timescale using scanning and transmission electron (TEM) microscopies. We conclude with a brief discussion of challenges and opportunities in future experiments involving this platform.

KEYWORDS
drug delivery, nanotube, porous silicon, RNA therapy, transfection

1 | INTRODUCTION

Nanostructured silicon, typically of a mesoporous morphology, continues to draw extensive attention as a therapeutic material capable of drug delivery,[1–5] including sophisticated multistage opportunities for therapy[5,6] that include cellular transfection.[7–9] Moving beyond microparticles of random orientation, more complex designs have emerged with an ongoing emphasis on the role of morphology in treatment efficacy.[4,10] Such morphologies include discrete discoidal particles,[11] square-shaped nanoparticles,[12] and one-dimensional nanowires/nanotubes,[13–15] with concomitant surface chemistry[16] to facilitate targeting and alter drug carrier resorption as required.

We have recently introduced straightforward routes to one-dimensional silicon nanotubes (SiNTs) that provide diverse opportunities in topics ranging from fundamental investigations of cell-structure interfaces (for isolated nanotubes[17]) to nanotube bundles that spatially resemble discoidal structures formed by more complex lithographic patterning.[14,18] Our sacrificial templating

approach, based on Si deposition on ZnO nanowire templates and subsequent template removal and in concert with controlled sonication, represents a non-lithographic entry into such morphologies. While a broad range of Si wall thicknesses are possible with these nanotubes, we restrict our choices here to relatively thin sidewalls such that a porous character is retained (pSiNTs).[19]

This paper outlines our initial investigations into the ability of such NT bundles to mediate the transfection of small interfering RNA (siRNA) probes attached strategically to the silicon nanotube surface, into mammalian cells. Given the existing challenges associated with off-target effects when using nonviral approaches of nucleic acid delivery, the introduction of small interfering RNA provides a useful benchmark for comparison.[20,21] Platforms for the delivery of siRNA from other pSi morphologies/designs have been investigated previously. The Sailor group has highlighted a calcium ion precipitation strategy, in which formation of the calcium silicate (Ca_2SiO_4) shell occurs simultaneously with the entrapment of siRNA associated within pSi nanoparticles (NPs).[22] As a consequence not only is a high loading of siRNAs achieved (~20 wt%) but dissolution of the Si skeleton is also slowed down by the Ca_2SiO_4 shell in order to attain a sustained release of siRNAs from the pSi carriers. In the case of siRNA capable of silencing the endogenous gene peptidylprolyl isomerase B (PPIB), the Ca-modified -pSiNP-siPPIB structure containing 2 targeting peptide moeities effected a knockdown of 52.8% of PPIB gene activity in Neuro-2a (mouse neuroblastoma) cells relative to untreated controls.[22] Shen and colleagues have evaluated discoidal pSi particles with ideally favorable flow dynamics (i.e., more likely to marginate and reach the vessel walls), in delivery of siRNA targeting the ataxia telangiectasia mutated (ATM) gene in human breast cancer cells via a multistage vector approach, but knockdown efficiency was not reported.[23,24] Finally, Tong et al report a strategy involving pSiNPs functionalized with polyethyleneimine (PEI) that demonstrates knockdown of multidrug resistance-associated protein 1 (MRP1) expression in glioblastoma multiforme cells (GBM) by 30%;[25] subsequent studies adding targeting nanobodies onto the pSi surface via a polyethylene glycol (PEG) linker directed towards either the epidermal growth factor receptor (EGFR) or the prostate specific membrane antigen (PSMA) improved this MRP1 expression knockdown value to 74%.[26]

In this report, we specifically illustrate proof of concept knockdown using suitably-modified pSiNTs for the case of an Enhanced Green Fluorescent Protein (eGFP) platform in HeLa (cervical cancer) cells. The emphasis here involves direct visualization of the nanotube bundles associated with the cells using both SEM and confocal fluorescence imaging. As nanoscale drug delivery vehicles are expected to be resorbed in clinical use, we also look for SiNT bundle degradation during the above in vitro timescales, again with a reliance on electron microscopies. Finally, we conclude with a discussion of future opportunities and challenges associated with such structures.

2 | RESULTS AND DISCUSSION

2.1 | Generation of SiNT bundles from nanotube films

SiNTs with submicron lengths are selected for use here (governed by growth time of the initial ZnO nanowire template) for optimal cellular uptake and other related interactions. Formation of SiNT arrays from Si deposition and ZnO etching from the original ZnO template produces continuous films (Figure 1A) that are physically scraped from a given substrate *after* APTES functionalization. For size control of the average nanotube bundle, ultrasonication is employed, with the average value dictated by duration of the sonication event (Figure 1B). The sonication process does not create discrete singular nanotubes, but rather fragments a given array into smaller nanotube bundles possessing the same length as those of the arrays before fragmentation; the interconnecting open end structures are also preserved (Figure 1D,E). The duration of ultrasonic exposure does not need to be long; use of a 5 min sonication period produces most bundle widths of less than a micrometer (75%), with less than 2% of the bundles within 2–3 μm (Figure 1B). Shifting this period to 10 min creates a slightly higher percentage of submicron bundles (82%) (Figure 1B). It is necessary to point out that from SEM and TEM imaging (Figure S1), even being subjected to a relatively high sonication power for 10 min, almost all the particles still maintained the well-defined, intact nanotube structures as well as a porous morphology, suggesting negligible mechanical damage to the given nanotube structure.

2.2 | siRNA conjugation/release to/from amine-modified silicon nanotubes

As with other known pSi—siRNA platforms, a straightforward surface modification approach employing requisite amino alkyl functionalized alkoxysilanes such as aminopropyltriethoxysilane (APTES) is employed here to achieve electrostatic binding of the RNA to the SiNT bundle. A nanotube concentration-dependent conjugation efficiency (CE) and siRNA mass loading is observed, with values of 23.1% CE and 5% siRNA mass loading were

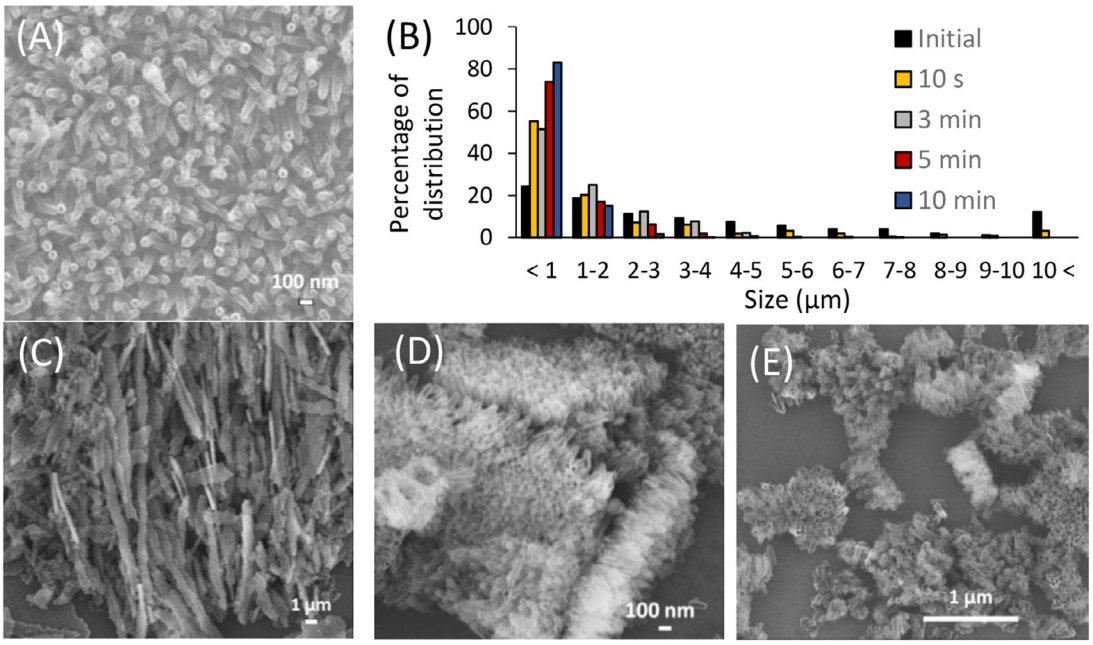

FIGURE 1 Top (plan) view SEM imaging showing the continuous film of SiNTs obtained after ZnO etching (A), histogram showing distribution of bundle sizes obtained after sonication for different time intervals (B), images of films obtained after scraping from the substrate (C), and bundles produced after sonication for 5 min (D) and 10 min (E).

TABLE 1 Conjugation efficiency and mass loading of siRNA to APTES-pSiNTs.

[APTES-pSiNTs]	CE%	% wt. conjugated siRNA
0.02 μg μL^{-1}	23.1 ± 4.7	5.0 ± 1.0
0.05 μg μL^{-1}	38.1 ± 8.3	3.3 ± 0.7
0.1 μg μL^{-1}	52.4 ± 7.3	2.3 ± 0.3

TABLE 2 Zeta potential measurements.

	Zeta potential (mV)
APTES-pSiNTs	+20.55 ± 0.35
siRNA/APTES-pSiNTs	−10.27 ± 0.26

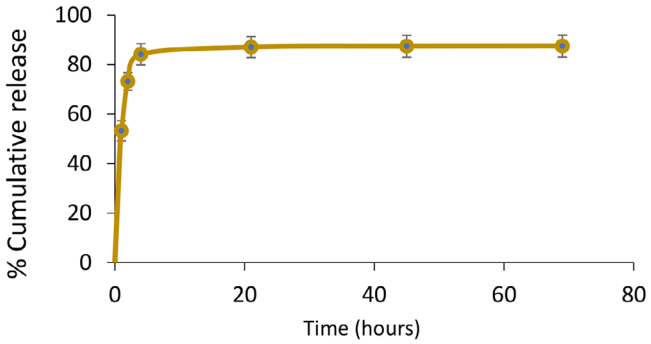

FIGURE 2 Release profile of FAM-labeled siRNA from APTES-pSiNTs.

achieved at the lowest concentration of APTES-pSiNTs (0.02 μg μL^{-1}) (Table 1). An aggregation of nanotube bundles is likely behind the observed enhanced %CE with increased APTES-pSiNTs concentration, since a decrease in % wt siRNA is presumably associated with lower surface areas and a reduction in the amino group density available for conjugating with siRNAs. Exposure of the APTES-pSiNTs to siRNA also results in a significant drop in zeta potential values of siRNA/APTES-pSiNTs due to the shielding of the amino groups by the negatively charged nucleic acids (Table 2). All these results point to the successful conjugation of siRNAs with the functionalized nanotubes.

Preliminary evaluation of siRNA release kinetics from the nanotube bundles was carried out using a fluorescently-labeled siRNA moiety (FAM-siRNA, λ_{em} = 520 nm, (FAM, a derivative of fluorescein)). A burst release was observed at 4 h post incubation (Figure 2). After this time point, most of the remaining siRNA was released over time. Although the cumulative release did not reach 100% (presumably due to a loss of a small amount of the material during washing and transfer), the release profile of siRNA from SiNTs was insignificantly affected.

The gradual disappearance of the brown functionalized pSiNT particles during the course of the release experiment is consistent with dissolution of SiNTs, thereby implying the possibility that siRNA release was mediated by the dissolution of the pSiNT matrix. We have subsequently investigated this in greater detail via scanning

and transmission electron microscopies (SEM;TEM) and is reported later on in this paper.

2.3 | Cytotoxicity assessment of APTES-pSiNTs

Since any nanoparticles can potentially exert adverse side effects on cell proliferation as well as transfection efficiency, in vitro cytotoxicity of APTES-pSiNTs was assessed. In this case, the viability of HeLa cells remained above 90% at all the tested doses after 36-h treatment, suggesting cytocompatibility of the NPs and the negligible influence of cell culture medium dilution on cell viability (Figure 2S).

2.4 | Interaction between siRNA/APTES-pSiNTs and HeLa cells

In order to evaluate feasibility of APTES-pSiNTs as nanocarriers in intracellular delivery of siRNA, a combination of imaging techniques was performed to assess cellular internalization of the nanotubes as well as the siRNA components.

2.4.1 | Brightfield imaging

Optical imaging of HeLa cells after 36-h transfection with siRNAs/APTES-pSiNTs showed a significant density of particles accumulating around the nuclei, thus indicating cellular association and possible internalization of the NTs inside the cells (Figure S3).

2.4.2 | Confocal microscopic imaging

In this study, delivery of the siRNA cargoes into HeLa cells was assessed by tracking fluorescently labeled siRNA. For transfection with free AF 647-siRNA, no extracellular fluorescent signal associated with siRNA was observed owing to instability of the cargoes in the extracellular environment (Figure 3A). Conversely, AF 647-siRNAs were shown to be associated with a considerable number of cells after 4 and 24 h transfection with AF 647-siRNA/APTES-pSiNTs (Figure 3D,E). Co-localization of the fluorescent siRNAs with the nanotube bundles (black spots located on cells (green channel, i.e., cell cytoplasm was labeled with Green BODIPY)) confirmed conjugation of siRNAs to the SiNT matrices. In addition, internalization of siRNA after 4 h was confirmed via confocal z-stack scanning (Figure S4). Therefore, the data presented here collectively provides evidence of the ability of SiNTs to immobilize, protect, and mediate delivery of siRNAs inside the cells. It is also necessary to point out that while both APTES-pSiNTs and the positive control Optifect were incubated with the same amount of siRNA, a greater concentration of siRNA was delivered by Optifect, presumably owing in part to a relatively higher CE.

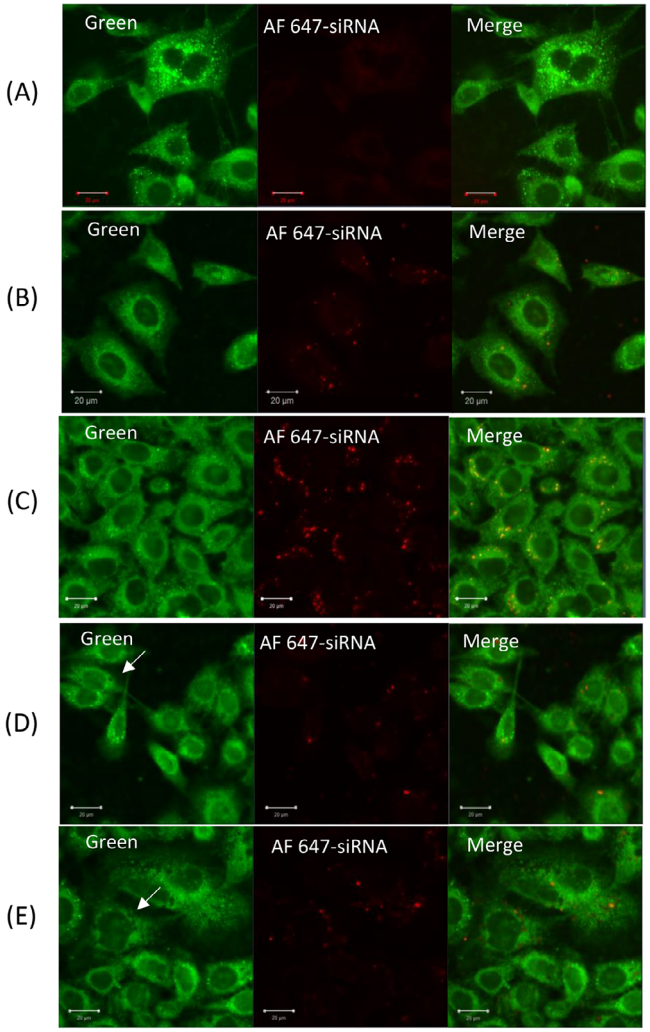

FIGURE 3 Confocal fluorescence imaging of HeLa cells (Green) and fluorescently labeled siRNA (AF 647, Red) without delivery vector (A), delivered using Optifect at 4 h (B) and 24 h post-transfection, (C) or delivered using APTES-pSiNTs at 4 h (D) and 24 h post-transfection (E). The arrows indicate the presence of the nanotube vectors. Scale bars: 20 μm.

2.4.3 | SEM imaging

While confocal imaging is a powerful tool to validate intracellular delivery of siRNAs, 2D SEM imaging provides additional information regarding the interface between siRNA/APTES-pSiNTs and cells.

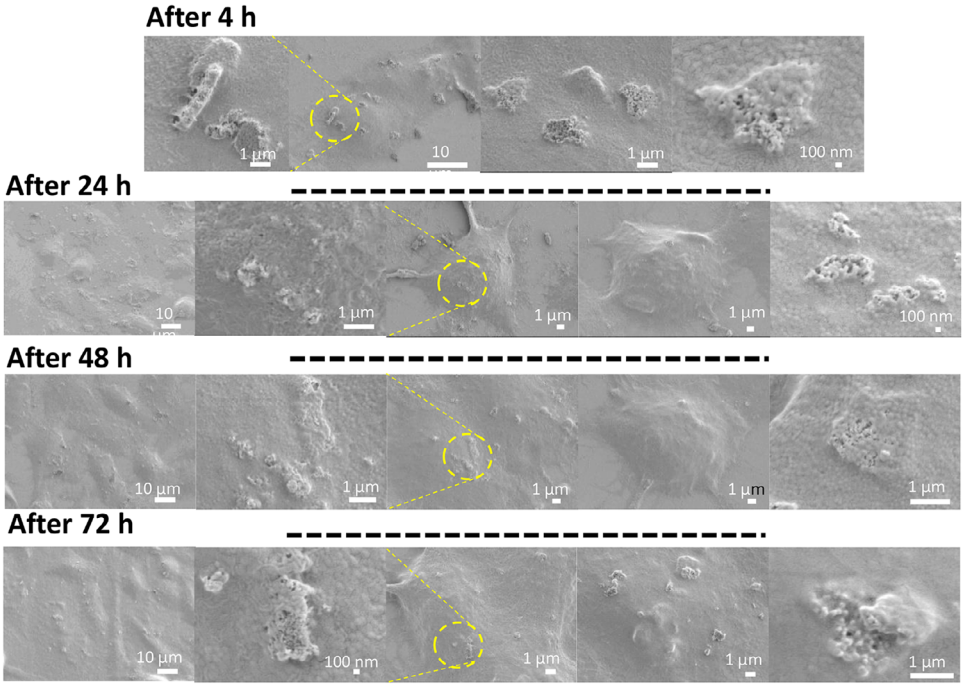

FIGURE 4 SEM images of HeLa cells after exposure to siRNA/APTES-pSiNTs for 4, 24, 48, and 72 h.

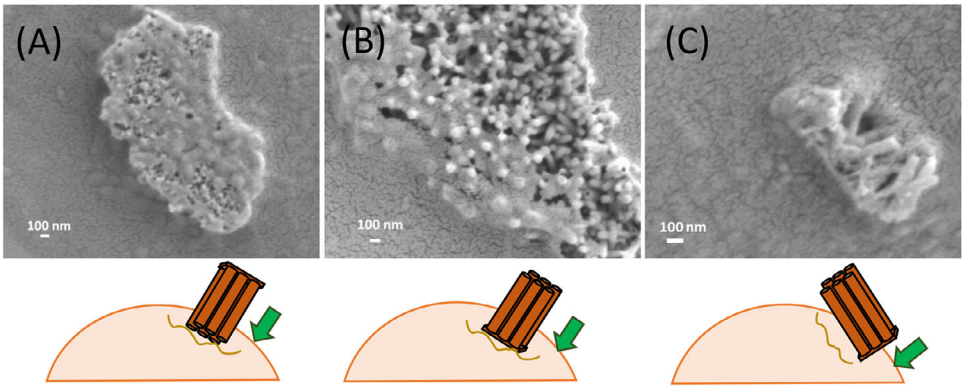

FIGURE 5 SEM imaging showing siRNA/APTES-pSiNT bundles positioned on the HeLa cells via: (A) closed-ends; (B) open ends, and (C) sideways orientation after 4-h incubation.

After 4-h transfection, the cell membrane was shown to wrap around the majority of the bundles. Even those within the largest size range (i.e., 4–5 μm) were also partially engulfed by cells at this time point (Figure 4). Based on SEM imaging, nanotube bundles can interact with cells via three main surfaces: (A) closed-end; (B) open-end; and (C) sideways (Figure 5). In all cases, the cell membrane appeared to favorably interact with all surfaces and readily wrap around the bundles. Since nanotubes were shown to almost fully penetrate the cell membrane after 4 h (Figure 5A,B), a relatively short nanotube length, that is, submicron height, is favorable for an optimal cellular uptake process.

At a 24-h time point, a large number of cells exhibited protruding surfaces, which was not observed in the untreated cells (Figures 4 and S5). The size and morphology of these visible protrusions are consistent with identification as nanotube bundles being enclosed within the cell membrane. Interestingly, the density of the protrusions continued to increase after 48 and 72 h, thereby implying successful internalization of a high concentration of the nanotubes. Presumably due to variation in the

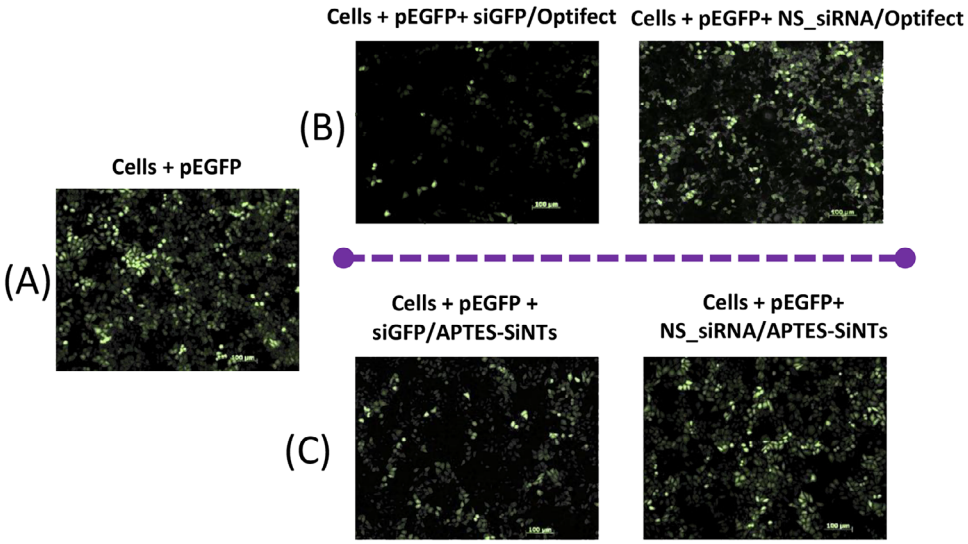

FIGURE 6 Fluorescent imaging of HeLa cells after transfection pEGFP (A) and subsequently with siGFP (or NS_siRNA) delivered by Optifect (control) (B) or APTES-pSiNTs (C). Scale bars: 100 μm.

intracellular pH as well as limited surface exposure of the bundles to the growth medium after membrane wrapping, the degradation of SiNT matrices slowed down as nanotube remnants were observed after 72 h.

2.5 | Silencing of eGFP expression in HeLa cells by delivery of siGFP

In the next set of studies, the ability of APTES-pSiNTs to deliver siGFP was evaluated. Cells expressing a plasmid containing the enhanced Green Fluorescent Protein gene (pEGFP) were subsequently treated as described below. Based on fluorescence imaging and quantification of eGFP expression, a 50% reduction in eGFP protein level was observed after nanotube-mediated delivery of siGFP (3–4 pmol). As a control non-specific siRNA conjugated to APTES-pSiNTs (NS_siRNA/APTES-pSiNT) were used. These insignificantly affected eGFP expression. Down-regulation of eGFP was therefore specifically induced by siGFP delivered by APTES-pSiNTs rather than the nanotube matrices themselves (Figures 6 and 7).

Although a higher percent knockdown of eGFP was observed in the case of the commercial Optifect transfection reagent (~80%–90%), it should be pointed out that a total amount of 10 pmol siGFP were conjugated to Optifect. This is assumed to be the maximum siRNA loading of Optifect since a complex formation with a higher siGFP density (100 pmol) did not yield a significant increase in eGFP knockdown.

With regard to NS_siRNA/Optifect, the level of eGFP knockdown varied randomly among trials (i.e., a large

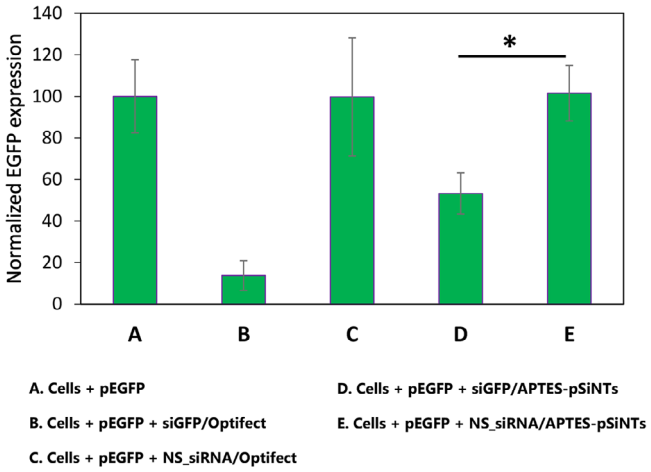

FIGURE 7 Normalized EGFP expression after 36-h siRNA transfection based on quantification of fluorescence intensity. *$p < 0.05$ ($n = 4$).

standard deviation). Since this significant fluctuation was not observed in siGFP/Optifect, this effect was not triggered by Optifect alone, but rather due to the off-target effects of NS_siRNAs, which have been reported to imperfectly bind to other mRNAs and potentially induce inflammatory responses.[27] While this off-target effect was not prominent in the case of NS_siRNA/APTES-pSiNTs, it was presumably due to a lower density of the NS_siRNA available ($n_{siRNA\ (conjugated)} = 3–4$ pmol).

The above knockdown value for the eGFP/pSiNT system is comparable to or better than some (but not all) other known values for pSi-based delivery systems from the literature as described in the Introduction section above.

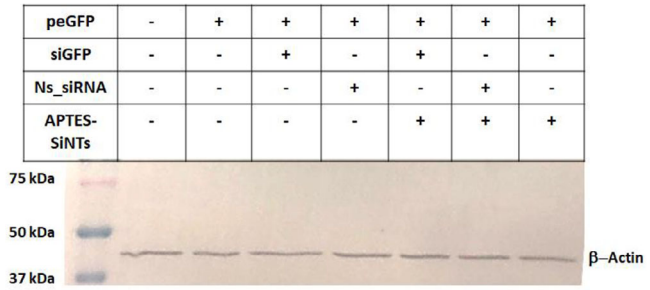

FIGURE 8 β-actin expression level in HeLa cells for the various combinations of treatments examined in this work.

2.6 | β-actin expression

Housekeeping proteins are involved in basic cellular maintenance and found in great abundance in many cell types.[28] Here, evaluation of the expression level of some proteins such as cytoskeletal β-actin, which are essential for cell motility and structural integrity,[29] is useful for assessment of the effect of a given treatment towards normal cellular functions. In this study described here, analysis of the β-actin protein by Western blot suggested that the transfection conditions as well as the APTES-pSiNT matrix itself do not significantly alter the level of β-actin protein, thus confirming specificity of the siGFP-mediated knockdown of eGFP and cytocompatibility of the nanotube matrices (Figure 8).

2.7 | Dissolution of siRNA/APTES-pSiNTs

Since understanding the biofate of the delivery vectors after completing their functions is essential to assess potential health risks imposed by long-term accumulation, evaluation of the degradability of APTES-pSiNTs after siRNA transfection experiments is necessary. Here, we use both SEM and TEM to evaluate the evolution of the APTES-modified pSiNT morphology before and after 36 h exposure to in vitro conditions (37°C, growth medium, both with and without the presence of the siRNA moiety + cells).

In these experiments, cell culture medium is used at physiological temperature to more closely mimic the behavior of the biological system, as demonstrated previously for pSi resorption measurements.[30,31] As a control we begin with an examination via SEM imaging of as-prepared (or unmodified (U))-pSiNTs after 6-h incubation in growth medium where enlarged pores appear on the nanotube surface, thus indicating signs of degradation. After 24 h, not only did pores presented on the remaining tubes became larger, but the well-defined nanotube geometry of almost all the tubes also completely collapsed, leaving behind the hollow structures as remnants (Figure S6A). Similar to these U-pSiNTs, numerous pores appear on the surface of APTES-pSiNTs, but relatively fewer in number and slightly smaller in size. These differences in structural changes as a function of surface chemistry for a given medium likely stems from the likely presence of a silica—derivative layer formed by condensation of APTES molecules that slightly increased the shell thickness, thereby inhibiting diffusion of the medium and slowing down dissolution of the functionalized nanotube surface.

Complementary TEM measurements reveal some fusion and aggregation of the nanotube bundles during this time window (Figure S7A,B); however, examination of the morphology in the presence of the eGFP siRNA and HeLa cells after 36 h is consistent with extensive degradation of well-defined nanotube bundles, as only remnants of nanotubes are visible, apparently embedded in a solid aggregate of undefined composition (Figure S7C). While not definitive, the presence of such structures are consistent with dissolution of the nanocarriers during the delivery of siRNAs in biological media.

3 | CONCLUSIONS

These studies highlight the ability of free-standing pSiNTs to serve as nanocarriers for delivery of siRNAs. Delivery of siGFP was assisted by APTES-pSiNTs, and eGFP protein expression (in HeLa cells) was reduced by 50%. While such initial results are encouraging, enhancement of delivery efficacy and understanding the delivery mechanism (e.g. cellular uptake pathways) operative in these systems in greater detail are imperative investigations moving forward. Improving CE and/or loading percent are critical additional steps to generation of an even more competitive siRNA delivery platform.

Overall, the studies presented here have demonstrated an exciting potential for sacrificial template-derived SiNT-based technology in nanomedicine, thereby expanding the library of possible nanostructures of Si in therapeutic delivery. While current studies typically involve nanotubes in bundle form, delivery studies focusing on discrete immobilized nanotubes are also of interest.

Since particle aggregation and multiple biological barriers impose critical challenges in therapeutic delivery, strategic designs of SiNT-based platforms that critically address these hurdles, along with scale-up production of these nanotubes, are of utmost importance if opportunities for future clinical translation are to be realized.

4 | EXPERIMENTAL SECTION/METHODS

4.1 | Cell culture

HeLa cervical cancer cells were maintained in Dulbecco's modified Eagles medium (DMEM) supplemented with 10% heat-inactivated fetal bovine serum (FBS), penicillin (88 U mL^{-1}), streptomycin (88 μg mL^{-1}), glutamine (0.88 mM) and 1/100 minimum essential medium (MEM) non-essential amino acids. Cells were maintained at 37°C with 5% CO_2 in air, in a humidified incubator. Cells were passaged into new flasks when they reached 80%–90% confluence at a dilution of 1:10.

4.2 | Preparation of SiNTs/APTES-pSiNTs

The starting material, SiNT arrays, were prepared from ZnO nanowire templates on FTO substrates, followed by Si deposition (using 0.5% SiH_4 in He) and ZnO template removal as described in detail elsewhere.[32,33] APTES-pSiNTs were subsequently prepared by exposure of a given nanotube array to a dilute solution of 2% APTES for 4 h at room temperature (RT) with constant stirring (120 rpm). After incubation, the substrates were washed with toluene and acetone, dried in air.[32] The NT arrays were gently scraped off from the surface of the substrate, sterilized, and fractured for 5 min (delivery of siEGFP) in diethyl pyrocarbonate (DEPC)-treated water (IBI Scientific) by ultrasonication.

4.3 | Preparation of siRNA/APTES-pSiNTs

The sonicated samples were further diluted with DEPC-treated water to obtain the target concentrations. APTES-pSiNTs were incubated with siRNAs [nonspecific siRNA (NS_siRNA), siGFP (Thermo Fisher Scientific) for 30 min at RT (~25°C).

4.4 | Characterization of siRNA/APTES-pSiNTs

4.4.1 | Zeta potential measurements

All zeta potential measurements were recorded using a Brookhaven Instruments unit with samples prepared according to procedures described previously.[32] After siRNA conjugation, the sample was centrifuged (13000 rpm, 10 min, 4°C), and the supernatant was collected. The nanoparticle pellet was washed twice and re-dispersed in ultrapure H_2O (2 mL). The sample was briefly ultrasonicated (~10 s) in the ice bath and the zeta potential values were collected at RT (10 runs, 30 cycles/run and fit to a Smoluchowski model. The Zeta potential of APTES-pSiNTs stock solution was also collected to evaluate changes in zeta potential before and after siRNA binding.

4.4.2 | Conjugation efficiency of siRNA to APTES-pSiNTs

The sonicated APTES-pSiNTs were diluted in DEPC-treated water to obtain the following concentrations: 0.02, 0.05, and 0.1 μg μL^{-1}, 145 μL, and the solutions were mixed with the same volume of siRNA stock (30 pmol, 5 μL) for 30 min at RT. The samples were centrifuged (13,300 rpm, 15 min, 4°C), and the concentration of the unbound siRNA was analyzed by using a Nanodrop UV-Vis spectrophotometer. The conjugation efficiency (% CE) and % mass loading were determined according to the following equations:

$$\%\ \mathrm{CE} = \frac{m_{siRNA\ (Stock)} - m_{siRNA(Supernatant)}}{m_{siRNA\ (stock)}} \times 100\% \quad (1)$$

$$\%\ \mathrm{Mass\ loading} = \frac{m_{siRNA}}{m_{siRNA} + m_{APTES-pSiNTs}} \times 100\% \quad (2)$$

4.4.3 | Release kinetics of siRNA from APTES-pSiNTs

APTES-pSiNTs (20 μg, 0.05 μg μL^{-1}) were incubated with fluorescent FAM-labeled siRNA (80 pmol) (Ex/Em: 485/520) for 30 min at RT, and the sample was centrifuged at 4°C (13,300 rpm, 10 min). The pellet was washed once with ultrapure water (200 μL), re-dispersed in PBS (400 μL), and incubated in the humidified incubator at 37°C with 5% CO_2 in air. At the time points indicated, the sample was centrifuged (13,000 rpm, 10 min, 4 oC) to collect the supernatant, and the pellet was re-dispersed in fresh PBS (400 μL). Two calibration curves were constructed using FAM-siRNA diluted in RNAse-free H_2O and PBS to determine mass loading and cumulative release of siRNA (Figure 2). Fluorescence readings were recorded using a microplate reader (Ex/Em 485/520).

4.4.4 | Interaction of siRNA/APTES-pSiNTs with HeLa cells

Exposure of HeLa cells with siRNA/APTES-pSiNTs was evaluated with a combination of brightfield imaging, confocal fluorescence imaging, and scanning electron microscopy according to detailed protocols outlined in supporting information.

4.5 | In vitro delivery of siRNA targeting EGFP-mRNA

4.5.1 | Cytotoxicity of APTES-pSiNTs

HeLa cells were seeded at a density of 5000 cells/well (100 μL complete medium) in a 96-well plate and were incubated at 37°C, 5% CO_2 for 24 h. Next day, to mimic siRNA delivery experiments, the reduced serum medium (Opti-MEM, 50 μL) was added into each well followed by different concentrations of APTES-pSiNTs (50 μL) prepared in sterilized water. The final concentrations of APTES-pSiNTs in the well are: 2.5, 5.0, 12.5, 17.5, 25, 35, and 50 μg mL^{-1}. Cells with no nanoparticle treatment served as the control. Cells were incubated for 36 h, and cell viability was assessed by CellTiter-Glo assays.

4.5.2 | Silencing eGFP expression in HeLa cells transiently transfected with pEGFP

In this experiment, HeLa cells were transiently transfected with plasmid encoding enhanced green fluorescent protein (pEGFP) and subsequently transfected with siGFP to suppress eGFP expression. For the negative control, cells were transfected with NS_siRNA. Details of these manipulations are provided in supporting information.

4.6 | Analysis of β-actin expression

Influence of siRNA transfection conditions to a housekeeping gene expression, in this case, β-actin, was analyzed by Western blot analysis, the details of which are described in supporting information.

4.7 | Dissolution of siRNA/APTES-pSiNTs

Cell lysates remaining after eGFP knockdown experiments were collected, centrifuged, and washed with DI H_2O. The pellets were re-dispersed in DI H_2O and the morphology of the NPs was evaluated by placing an ~10 μL drop on carbon-coated Cu grids and analyzing them via transmission electron microscopy (TEM) (JEOL JEM-2100 operating at 200 kV).

ACKNOWLEDGMENTS

The authors gratefully acknowledge the Robert A. Welch Foundation (Grant P-1212) for their financial support of this research.

CONFLICT OF INTEREST STATEMENT

The authors declare no conflicts of interest.

DATA AVAILABILITY STATEMENT

The data that support the findings of this study are available from the corresponding author upon reasonable request.

ORCID

Jeffery L. Coffer https://orcid.org/0000-0003-0267-9646

REFERENCES

1. L. T. Canham, in *Porous Silicon for Biomedical Applications* (Ed.: H. A. Santos), Woodhead Publishing, Cambridge, UK, **2014**, pp. 3.
2. X. Li, J. St. John, J. L. Coffer, Y. Chen, R. F. Pinizzotto, J. Newey, C. Reeves, L. T. Canham, *Biomed. Microdevices* **2000**, *2*, 265.
3. J. Salonen, in *Handbook of Porous Silicon* (Ed.: L. Canham), Springer International Publishing, Cham, **2018**, pp. 1377.
4. W. Li, Z. Liu, F. Fontana, Y. Ding, D. Liu, J. T. Hirvonen, H. A. Santos, *Adv. Mater.* **2018**, *30*, 1703740.
5. Y. Xue, H. Bai, B. Peng, T. Tieu, J. Jiang, S. Hao, P. Li, M. Richardson, J. Baell, H. Thissen, A. Cifuentes, L. Li, N. H. Voelcker, *Adv. Healthc. Mater.* **2022**, *11*, 2200076.
6. F. Fontana, M.-A. Shahbazi, D. Liu, H. Zhang, E. Mäkilä, J. Salonen, J. T. Hirvonen, H. A. Santos, *Adv. Mater.* **2017**, *29*, 1603239.
7. J. Joo, E. J. Kwon, J. Kang, M. Skalak, E. J. Anglin, A. P. Mann, E. Ruoslahti, S. N. Bhatia, M. J. Sailor, *Nanoscale Horiz.* **2016**, *1*, 407.
8. B. Kim, S. Sun, J. A. Varner, S. B. Howell, E. Ruoslahti, M. J. Sailor, *Adv. Mater.* **2019**, *31*, 1902952.
9. E. Maurizi, D. A. Martella, D. Schiroli, A. Merra, S. A. Mustfa, G. Pellegrini, C. Macaluso, C. Chiappini, *Adv. Sci.* **2022**, *9*, 2203257.
10. A. B. Jindal, *Int. J. Pharm.* **2017**, *532*, 450.
11. B. Godin, C. Chiappini, S. Srinivasan, J. F. Alexander, K. Yokoi, M. Ferrari, P. Decuzzi, X. Liu, *Adv. Funct. Mater.* **2012**, *22*, 4225.
12. Z. Qin, J. Joo, L. Gu, M. J. Sailor, *Part. Part. Syst. Charact.* **2014**, *31*, 252.
13. C. Chiappini, J. O. Martinez, E. De Rosa, C. S. Almeida, E. Tasciotti, M. M. Stevens, *ACS Nano* **2015**, *9*, 5500.
14. X. Huang, R. Gonzalez-Rodriguez, R. Rich, Z. Gryczynski, J. L. Coffer, *Chem. Commun.* **2013**, *49*, 5760.
15. S. Gopal, C. Chiappini, J. Penders, V. Leonardo, H. Seong, S. Rothery, Y. Korchev, A. Shevchuk, M. M. Stevens, *Adv. Mater.* **2019**, *31*, 1806788.

16. M. J. Sailor, in *Handbook of Porous Silicon* (Ed.: L. Canham), Springer International Publishing, Cham, **2018**, pp. 513.
17. R. Elnathan, M. G. Barbato, X. Guo, A. Mariano, Z. Wang, F. Santoro, P. Shi, N. H. Voelcker, X. Xie, J. L. Young, Y. Zhao, W. Zhao, C. Chiappini, *Nat. Rev. Mater.* **2022**, *7*, 953.
18. N.T. Le, Y. Tian, R. Gonzalez-Rodriguez, L. J. Coffer, *Pharmaceutics* **2019**, *11*, 571.
19. N. T. Le, J. L. Coffer, in *Semiconducting Silicon Nanowires for Biomedical Applications*, 2nd ed., (Ed.: J. Coffer), Woodhead Publishing, Cambridge, UK, **2022**, pp. 207.
20. K. Tatiparti, S. Sau, S. K. Kashaw, A. K. Iyer, *Nanomaterials* **2017**, *7*, 77.
21. F. Mainini, M. R. Eccles, *Molecules* **2020**, *25*, 2692.
22. J. Kang, J. Joo, E. J. Kwon, M. Skalak, S. Hussain, Z.-G. She, E. Ruoslahti, S. N. Bhatia, M. J. Sailor, *Adv. Mater.* **2016**, *28*, 7962.
23. H. Shen, C. Rodriguez-Aguayo, R. Xu, V. Gonzalez-Villasana, J. Mai, Y. Huang, G. Zhang, X. Guo, L. Bai, G. Qin, X. Deng, Q. Li, D. R. Erm, B. Aslan, X. Liu, J. Sakamoto, A. Chavez-Reyes, H.-D. Han, A. K. Sood, M. Ferrari, G. Lopez-Berestein, *Clin. Cancer Res.* **2013**, *19*, 1806.
24. M. Zhang, R. Xu, X. Xia, Y. Yang, J. Gu, G. Qin, X. Liu, M. Ferrari, H. Shen, *Biomaterials* **2014**, *35*, 423.
25. W. Y. Tong, M. Alnakhli, R. Bhardwaj, S. Apostolou, S. Sinha, C. Fraser, T. Kuchel, B. Kuss, N. H. Voelcker, *J. Nanobiotechnology* **2018**, *16*, 38.
26. T. Tieu, M. Wojnilowicz, P. Huda, K. J. Thurecht, H. Thissen, N. H. Voelcker, A. Cifuentes-Rius, *Biomater. Sci.* **2021**, *9*, 133.
27. A. L. Jackson, P. S. Linsley, *Nat. Rev. Drug Discov.* **2010**, *9*, 57.
28. R. E. Ferguson, H. P. Carroll, A. Harris, E. R. Maher, P. J. Selby, R. E. Banks, *PROTEOMICS* **2005**, *5*, 566.
29. V. Procaccio, G. Salazar, S. Ono, M. L. Styers, M. Gearing, A. Davila, R. Jimenez, J. Juncos, C.-A. Gutekunst, G. Meroni, B. Fontanella, E. Sontag, J. M. Sontag, V. Faundez, B. H. Wainer, *Am. J. Hum. Genet* **2006**, *78*, 947.
30. C. Chiappini, E. Tasciotti, J. R. Fakhoury, D. Fine, L. Pullan, Y.-C. Wang, L. Fu, X. Liu, M. Ferrari, *ChemPhysChem* **2010**, *11*, 1029.
31. J. O. Martinez, C. Chiappini, A. Ziemys, A. M. Faust, M. Kojic, X. Liu, M. Ferrari, E. Tasciotti, *Biomaterials* **2013**, *34*, 8469.
32. N. T. Le, Ph.D. Dissertation, Texas Christian University **2021**.
33. N. T. Le, G. R. Akkaraju, J. L. Coffer, *ACS Appl. Bio Mater.* **2020**, *3*, 208.

SUPPORTING INFORMATION

Additional supporting information can be found online in the Supporting Information section at the end of this article.

How to cite this article: N. Le, G. Akkaraju, J. L. Coffer, *Nano Select* **2024**, *5*, 2300111.
https://doi.org/10.1002/nano.202300111